J|A|C|S
ARTICLES
Published on Web 02/02/2007

Synthesis, Structure, and Magnetic Properties of Valence Ambiguous Dinuclear Antiferromagnetically Coupled Cobalt and Ferromagnetically Coupled Iron Complexes Containing the Chloranilate(2−) and the Significantly Stronger Coupling Chloranilate(•3−) Radical Trianion

Kil Sik Min,[†] Antonio G. DiPasquale,[‡] James A. Golen,[‡] Arnold L. Rheingold,[‡] and Joel S. Miller*,[†]

Contribution from Department of Chemistry, University of Utah, Salt Lake City, Utah 84112-0850, and the Department of Chemistry, University of California, San Diego, La Jolla, California 92093-0358

Received October 8, 2006; E-mail: jsmiller@chem.utah.edu

Abstract: Dinuclear $[(TPyA)M^{II}(CA^{2-})M^{II}(TPyA)]^{2+}$ [TPyA = tris(2-pyridylmethyl)amine; CA^{2-} = chloranilate dianion; M = Co ($\mathbf{1}^{2+}$), Fe ($\mathbf{2}^{2+}$)] complexes have been prepared by the reaction of $M(BF_4)_2{\cdot}6H_2O$, TPyA, H_2CA, and triethylamine in MeOH solution. Their reduced forms $[(TPyA)M^{II}(CA^{\bullet 3-})M^{II}(TPyA)]^{+}$ [M = Co($\mathbf{1}^{+}$), Fe ($\mathbf{2}^{+}$)] have been synthesized by using cobaltocene, and oxidized forms of **1**, $[(TPyA)Co^{III}(CA^{n})Co^{III}(TPyA)]^{z+}$ [$z = 3$, $n = 3-$ ($\mathbf{1}^{3+}$); $z = 4$, $n = 2-$ ($\mathbf{1}^{4+}$)], have been obtained by using $FcBF_4$ and $ThianBF_4$ (Fc = ferrocenium; Thian = thianthrinium), respectively. The dinuclear compound bridged chloranilates (CA^{2-} or $CA^{\bullet 3-}$) were isolated and characterized by X-ray crystallography, electrochemistry, magnetism, and EPR spectroscopy. Unlike the other redox products, valence ambiguous $\mathbf{1}^{3+}$ forms via a complex redox-induced valence electron rearrangement whereby the one-electron oxidation of the $[Co^{II}CA^{2-}Co^{II}]^{2+}$ core forms $[Co^{III}CA^{\bullet 3-}Co^{III}]^{3+}$, not the expected simple 1-e$^-$ transfer mixed-valent $[Co^{II}CA^{2-}Co^{III}]^{3+}$ core. The M ions in **1** and **2** have a distorted octahedral geometry by coordination with four nitrogens of a TPyA, two oxygens of a chloranilate. Due to the interdimer offset face-to-face $\pi-\pi$ and/or herringbone interactions, all complexes show extended 1-D and/or 2-D supramolecular structures. The existence of $CA^{\bullet 3-}$ in $\mathbf{1}^{3+}$ is confirmed from both solid-state magnetic and solution EPR data. Co-based $\mathbf{1}^{n+}$ exhibit antiferromagnetic interactions [$\mathbf{1}^{2+}$: $g = 2.24$, $J/k_B = -0.65$ K (-0.45 cm^{-1}); $\mathbf{1}^{+}$: $g = 2.36$, $J/k_B = -75$ K (52 cm^{-1})], while Fe-based $\mathbf{2}^{n+}$ exhibit ferromagnetic interactions [$\mathbf{2}^{2+}$: $g = 2.08$, $J/k_B = 1.0$ K (0.70 cm^{-1}); $\mathbf{2}^{+}$: $g = 2.03$, $J/k_B = 28$ K (19 cm^{-1})] [$H = -2J\mathbf{S}_1{\cdot}\mathbf{S}_2$ for $\mathbf{1}^{2+}$ and $\mathbf{2}^{2+}$; $H = -2J(\mathbf{S}_1{\cdot}\mathbf{S}_2 + \mathbf{S}_2{\cdot}\mathbf{S}_3)$ for $\mathbf{1}^{+}$ and $\mathbf{2}^{+}$]. Thus, due to direct spin exchange $CA^{\bullet 3-}$ is a much strong spin coupling linkage than the superexchange spin-coupling pathway provided by CA^{2-}.

Introduction

The design and synthesis of discrete metal complexes has enabled the structural elucidation of metalloenzymes[1] and development of redox catalysts,[2] as well as the understanding and development of spin-coupled materials.[3] In particular, coordination compounds containing 2,5-dichloro-3,6-dihydroxy-1,4-benzoquinonediide, chloranilate (CA^{2-}) as bis-bidentate ligands have been prepared and studied extensively,[4] because they have a delocalized π system that transmits electronic effects between the bridged M sites. In principle, upon either oxidation or reduction, CA^{2-} can form an organic radical ($S = {}^1/_2$), which should lead to strong spin coupling with paramagnetic species. Although numerous CA^{2-}-bridged dinuclear compounds have been synthesized, dinuclear complexes having the spin bearing chloranilate radical ligand ($CA^{\bullet 3-}$ or $CA^{\bullet -}$) have not been reported.

Some years ago, several valence ambiguous[5] dinuclear cobalt complexes prepared by the reaction of 2,5-dihydroxy-1,4-benzoquinone (H_2DHBQ) and its homologues as bridging ligands and $Co(BF_4)_2$, e.g., $[(tripod)Co(L)Co(tripod)]^{n+}$ [n =

[†] University of Utah.
[‡] University of California, San Diego.

(1) (a) Williams, N. H.; Cheung, W.; Chin, J. *J. Am. Chem. Soc.* **1998**, *120*, 8079. (b) Liaw, W.-F.; Lee, N.-H.; Chen, C.-H.; Lee, C.-M.; Lee, G.-H.; Peng, S.-M. *J. Am. Chem. Soc.* **2000**, *122*, 488. (c) Tshuva, E. Y.; Lippard, S. J. *Chem. Rev.* **2004**, *104*, 987.
(2) (a) Wada, T.; Tsuge, K.; Tanaka, K. *Inorg. Chem.* **2001**, *40*, 329. (b) Zilbermann, I.; Maimon, E.; Cohen, H.; Meyerstein, D. *Chem. Rev.* **2005**, *105*, 2609. (c) Poulsen, A. K.; Rompel, A.; McKenzie, C. J. *Angew. Chem., Int. Ed.* **2005**, *44*, 6916.
(3) (a) Hicks, R. G.; Lemaire, M. T.; Thompson, L. K.; Barclay, T. M. *J. Am. Chem. Soc.* **2000**, *122*, 8077. (b) Beckmann, Y.; Bill, E.; Weyhermüller, T.; Wieghardt, K. *Inorg. Chem.* **2003**, *42*, 1045. (c) Benelli, C.; Gatteschi, D. *Chem. Rev.* **2002**, *102*, 2369.
(4) (a) Kitagawa, S.; Kawata, S. *Coord. Chem. Rev.* **2002**, *224*, 11. (b) Kawahara, M.; Kabir, M. K.; Yamada, K.; Adachi, K.; Kumagai, H.; Narumi, Y.; Kindo, K.; Kitagawa, S.; Kawata, S. *Inorg. Chem.* **2004**, *43*, 92. (c) Nagayoshi, K.; Kabir, M. K.; Tobita, H.; Honda, K.; Kawahara, M.; Katada, M.; Adachi, K.; Nishikawa, H.; Ikemoto, I.; Kumagai, H.; Hosokoshi, Y.; Inoue, K.; Kitagawa, S.; Kawata, S. *J. Am. Chem. Soc.* **2003**, *125*, 221.
(5) Rittenberg, D. K.; Sugiura, K-i.; Sakata, Y.; Arif, A. M.; Miller, J. S. *Inorg. Chem.* **2001**, *40*, 3654.

10.1021/ja067208q CCC: $37.00

1, 2; tripod = 1,1,1-tris(diphenylphosphanomethyl)ethane ($CH_3C(CH_2PPh_2)_3$); L = deprotonated 1,2,4,5-tetrahydroxybenzene and 1,2,4,5-tetrahydroxy-3,6-dichlorobenzene, etc.], were reported.[6] Among them, two cobalt dimers are best described as $[(tripod)Co^{III}(DHBQ^{4-})Co^{III}(tripod)]^{2+}$ and $[(tripod)Co^{III}(CA^{4-})Co^{III}(tripod)]^{2+}$ via characterization by NMR, electrochemistry, and X-ray crystallography and are not $[(tripod)Co^{II}(DHBQ^{2-})Co^{II}(tripod)]^{2+}$ and $[(tripod)Co^{II}(CA^{2-})Co^{II}(tripod)]^{2+}$.[6] Reduction of these CA^{4-} related species with cobaltocene led to mixed-valent $[(tripod)Co^{II}(DHBQ^{4-})Co^{III}(tripod)]^{+}$ and $[(tripod)Co^{II}(CA^{4-})Co^{III}(tripod)]^{+}$, not $CA^{\bullet 3-}$ related species.[7]

In contrast, three dinuclear complexes bridged with $DHBQ^{\bullet 3-}$, i.e., $[(CTH)Fe^{III}(DHBQ^{\bullet 3-})Fe^{III}(CTH)](ClO_4)_3$,[8a] $[(CTH)Co^{III}(DHBQ^{\bullet 3-})Co^{III}(CTH)](PF_6)_3$,[8b] and $[(TPyA)Co^{III}(DHBQ^{\bullet 3-})Co^{III}(TPyA)](PF_6)_3$[8c] (CTH = *dl*-5,7,7,12,14,14-hexamethyl-1,4,8,-11-tetraazacyclotetradecane) have been reported. The former diiron complex exhibited a very strong antiferromagnetic interaction between the iron ion and the $DHBQ^{\bullet 3-}$ [8a] while the latter dicobalt complexes exhibited the so-called valence-tautomeric spin crossover behavior,[9] e.g., $Co^{III}(DHBQ^{\bullet 3-})Co^{III} \leftrightarrow Co^{II}(DHBQ^{2-})Co^{III}$ cores.[8b,c]

It should be noted that formation of these CA^{2-}-reduced, $CA^{\bullet 3-}$ related species[8] occurs via a complex induced electron-transfer reaction involving addition of an oxidant, not a reductant. This redox reaction can be described as a redox-induced electron rearrangement (RIER) whereby the one-electron oxidation of the $[M^{II}CA^{2-}M^{II}]^{2+}$ (M = Fe, Co) core forms $[M^{III}CA^{\bullet 3-}M^{III}]^{3+}$, not the expected mixed-valent $[M^{II}CA^{2-}M^{III}]^{3+}$ core. This RIER is related to the redox induced internal electron-transfer reactions with concomitant chemical rearrangements reported by Steifel and co-workers[10] and attributed to be the mechanistic pathway for hydrogen reduction by NiFe-hydrogenases.[11]

To develop the chemistry of $CA^{\bullet 3-}$ with the goal of preparing new materials with strong spin coupling and atypical magnetic behaviors, we report herein on the formation and characterization, with emphasis on the magnetic properties of a series of isostructural dicobalt and diiron complexes bridged by either the chloranilate dianion (CA^{2-}) or the trianion radical ($CA^{\bullet 3-}$) (Scheme 1) that has been preliminarily described in a communication.[12] Spin bearing $CA^{\bullet 3-}$ is expected to be a stronger spin coupling linkage than CA^{2-} as it can couple by direct exchange, not indirect superexchange for which can only occur for diamagnetic CA^{2-}.[13]

Scheme 1

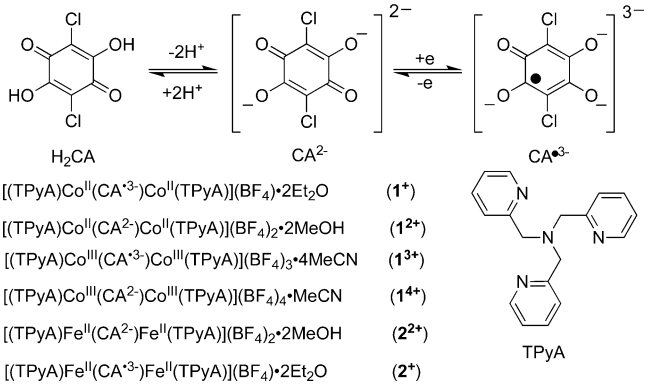

Experimental Section

All chemicals used in the synthesis were of reagent grade and used without further purification. Tris(2-pyridylmethyl)amine (TPyA),[14a] thianthrinium tetrafluoroborate ($ThianBF_4$),[14b] and $[(TPyA)Co^{II}(DHBQ^{2-})Co^{II}(TPyA)](BF_4)_2$[8c] were prepared according to literature procedures. Ferrocenium tetrafluoroborate ($FcBF_4$) and cobaltocene ($CoCp_2$) were used as received from Aldrich. Solvents were distilled from the appropriate drying agents under nitrogen before use. All syntheses were performed in a wet or dry oxygen-free (<1 ppm O_2) box. Infrared spectra were recorded with a Bruker Tensor 37 FT−IR spectrophotometer (±1 cm^{-1}). UV/vis spectra were recorded with an Ocean Optics HR2000 high-resolution spectrophotometer. Cyclic voltammograms were performed using an EPSILON electrochemistry analyzer in MeCN or CH_2Cl_2 [0.1 M $[(n\text{-}Bu)_4N]BF_4$ supporting electrolyte] at a scan rate of 100 mV s^{-1} using a Pt working electrode vs ferrocenium/ferrocene (Fc^+/Fc) with Fc as an internal standard, and the data are reported vs the SCE. Elemental analyses were performed by Complete Analysis Laboratories, Inc. or Chemisar Laboratories. Magnetic susceptibilities were measured in applied fields of 300, 5000, and 10 000 Oe between 2 and 300 K on a Quantum Design MPMS superconducting quantum interference (SQUID) magnetometer as previously reported.[15] Diamagnetic corrections were made by using Pascal's constants. X-Band EPR spectra were recorded on a Bruker EMX-EPR spectrometer. The spectra were simulated by iteration of the isotropic *g* values, hyperfine coupling constants, and line widths using the WINEPR SimFonia program.[16]

$[(TPyA)Co^{II}(CA^{2-})Co^{II}(TPyA)](BF_4)_2$·2MeOH ($1^{2+}$). To a MeOH solution (10 mL) of $Co(BF_4)_2$•$6H_2O$ (234 mg, 0.688 mmol) were added a MeOH solution (10 mL) of TPyA (200 mg, 0.688 mmol) and a MeOH solution (10 mL) of chloranilic acid (H_2CA, 72 mg, 0.344 mmol) in a wet box (<1 ppm O_2), and the color became dark red and then dark red-brown. Triethylamine (0.1 mL, 0.688 mmol) was added to the mixture for neutralization, which gives rise to a red-brown solution, and the solution was heated to reflux for 30 min. After standing at room temperature overnight, dark red-brown crystals formed that were collected by filtration, washed with methanol, and dried in vacuo to afford 257 mg (65%) of $\mathbf{1}^{2+}$. Anal. Calcd for $C_{44}H_{44}B_2Cl_2Co_2F_8N_8O_6$: C, 46.22; H, 3.88; N, 9.80. Found: C, 46.25; H, 3.85; N, 9.96. FT−IR (KBr): ν_{CH} 3082 (w), 2919 (w), 1609 (s), ν_{CO} 1526 (vs), 1484 (s), 1438 (s), 1379 (s), 1291 (m), 1060 (multiple, br), 851 (s), 771 (s) cm^{-1}. Absorption spectrum (CH_2Cl_2), λ_{max}, cm^{-1}/nm (ϵ_M, L mol^{-1} cm^{-1}): 25 640/390(5.5×10^3), 18 620/537(8.3×10^2).

(6) Heinze, K.; Huttner, G.; Zsolnai, L.; Jacobi, A.; Schober, P. *Chem.—Eur. J.* **1997**, *3*, 732.
(7) Heinze, K.; Huttner, G.; Walter, O. *Eur. J. Inorg. Chem.* **1999**, 593.
(8) (a) Dei, A.; Gatteschi, D.; Pardi, L.; Russo, U. *Inorg. Chem.* **1991**, *30*, 2589. (b) Carbonera, C.; Dei, A.; Létard, J.-F.; Sangregorio, C.; Sorace, L. *Angew. Chem., Int. Ed.* **2004**, *43*, 3136. (c) Tao, J.; Maruyama, H.; Sato, O. *J. Am. Chem. Soc.* **2006**, *128*, 1790.
(9) (a) Shultz, D. A. In *Magnetism - Molecules to Materials*; Miller, J. S., Drillon, M., Eds.; Wiley-VCH: Mannheim, 2001; Vol. 2, p 281. (b) Dei, A.; Gatteschi, D.; Sangregorio, C.; Sorace, L. *Acc. Chem. Res.* **2004**, *37*, 827.
(10) (a) Wang, K.; McConnachie, J. M.; Stiefel, E. I. *Inorg. Chem.* **1999**, *38*, 4334. (b) McConnachie, J. M.; Stiefel, E. I. *Inorg. Chem.* **1997**, *36*, 6144. (c) Murray, H. H.; Wei, L.; Sherman, S. E.; Greaney, M. A.; Eriksen, K. A.; Carstensen, B.; Halbert, T. R.; Stiefel, E. I. *Inorg. Chem.* **1995**, *34*, 841. (d) Pan, W.-H.; Harmer, M. A.; Halbert, T. R.; Stiefel, E. I. *J. Am. Chem. Soc.* **1984**, *106*, 459. (e) Wei, L.; Halbert, T. R.; Murray, H. H.; Stiefel, E. I. *J. Am. Chem. Soc.* **1990**, *112*, 6431.
(11) Maroney, M. J.; Brynegelson, J. *Biol. Inorg. Chem.* **2001**, *6*, 453.
(12) Min, K. S.; Rheingold, A. L.; DiPasquale, A.; Miller, J. S. *Inorg. Chem.* **2006**, *45*, 6135.
(13) Anderson, P. W. *Phys. Rev.* **1950**, *79*, 350. Anderson P. W. *Phys. Rev.* **1959**, *115*, 2. Anderson P. W. Exchange in Insulators: Superexchange, Direct Exchange, and Double Exchange. In *Magnetism*; Rado, G. T., Shuhl, H., Eds.; Academic Press: New York, 1963; p 67. Goodenough, J. B. *Phys. Chem. Solids* **1958**, *6*, 287. Goodenough, J. B. *Phys. Rev.* **1955**, *100*, 504. Kanamori, J. *Phys. Chem. Solids* **1959**, *10*, 87.
(14) (a) Tyeklár, Z.; Jacobson, R. R.; Wei, N.; Murthy, N. N.; Zubieta, J.; Karlin, K. D. *J. Am. Chem. Soc.* **1993**, *115*, 2677. (b) Boduszek, B.; Shine, H. J. *J. Org. Chem.* **1988**, *53*, 5142.
(15) Brandon, E. J.; Rittenberg, D. K.; Arif, A. M.; Miller, J. S. *Inorg. Chem.* **1998**, *37*, 3376.
(16) *WINEPR SimFonia*, v. 1.2; Bruker Instruments, Inc.: 1995.

[(TPyA)Co^{II}(CA$^{\bullet 3-}$)Co^{II}(TPyA)](BF$_4$)·2Et$_2$O (1$^+$). To an MeCN solution (5 mL) of **1**$^{2+}$ (50 mg, 0.044 mmol) was added an MeCN solution (5 mL) of $CoCp_2$ (8.3 mg, 0.044 mmol) in a dry box (<1 ppm O_2). The color turned dark red, and the mixture was stirred for 1 h at room temperature. Red-brown block-shaped crystals of **1**$^+$ were obtained by diffusion of diethyl ether into the reaction mixture of acetonitrile for 2 or 3 days and were collected by filtration, washed with MeCN, and dried in vacuo (yield: 40 mg, 80%). Anal. Calcd for $C_{42}H_{36}BCl_2Co_2F_4N_8O_4$: C, 50.83; H, 3.66; N, 11.29. Found: C, 50.36; H, 3.95; N, 11.01. FT−IR (KBr): ν_{CH} 3065 (w), 2926 (w), 1604 (s), 1534 (w), 1481 (s), ν_{CO} 1442 (vs), 1264 (m), 1055 (multiple, br), 832 (s), 773 (s) cm^{-1}. Absorption spectrum (MeCN), λ_{max}, cm^{-1}/nm (ϵ_M, L mol^{-1} cm^{-1}): 40 500/247(1.8×10^4), 30 300/330(1.2×10^4), 20 660/484(6.8×10^3), 17 800/562(sh, 3.3×10^3), 13 550/738(2.5×10^3).

[(TPyA)Co^{III}(CA$^{\bullet 3-}$)Co^{III}(TPyA)](BF$_4$)$_3$·4MeCN (1^{3+}). To an MeCN solution (5 mL) of **1**$^{2+}$ (51 mg, 0.045 mmol) was added an MeCN solution (3 mL) of $FcBF_4$ (13 mg, 0.045 mmol) in a dry box (<1 ppm O_2). The color turned dark red, and the solution was stirred for 1 h at room temperature. Dark red block-shaped crystals of **1**$^{3+}$ were obtained by diffusion of diethyl ether into the reaction mixture of acetonitrile for 2 or 3 days and were collected by filtration, washed with MeCN, and dried in vacuo (yield: 42 mg, 71%). Anal. Calcd for $C_{42}H_{36}B_3Cl_2Co_2F_{12}N_8O_4$: C, 43.26; H, 3.11; N, 9.61. Found: C, 43.55; H, 3.40; N, 9.50. FT−IR (KBr): ν_{CH} 3117 (w), 2994 (w), 1611 (s), 1539 (s), 1490 (s), ν_{CO} 1421 (vs), 1292 (s), 1051 (multiple, br), 867 (m), 770 (s) cm^{-1}. Absorption spectrum (MeCN), λ_{max}, cm^{-1}/nm (ϵ_M, L mol^{-1} cm^{-1}): 39 840/251 (4.5×10^4), 29 150/343 (3.0×10^4), 19 400/516 (1.6×10^3).

[(TPyA)Co^{III}(CA^{2-})Co^{III}(TPyA)](BF$_4$)$_4$·MeCN (1^{4+}). To an MeCN solution (5 mL) of **1**$^{2+}$ (50 mg, 0.044 mmol) was added an MeCN solution (5 mL) of $ThianBF_4$ (27 mg, 0.088 mmol) in a dry box (<1 ppm O_2). The color turned dark brown, and the solution was stirred for 1 h at room temperature. Dark brown block-shaped crystals of **1**$^{4+}$ were obtained by diffusion of diethyl ether into the reaction mixture of acetonitrile for 2 or 3 days and were collected by filtration, washed with MeCN, and dried in vacuo (yield: 46 mg, 81%). Anal. Calcd for $C_{42}H_{36}B_4Cl_2Co_2F_{16}N_8O_4$: C, 40.27; H, 2.90; N, 8.94. Found: C, 40.32; H, 3.19; N, 9.16. FT−IR (KBr): ν_{CH} 3119 (w), 2995 (w), 1613 (s), ν_{CO} 1513 (vs), 1449 (s), 1378 (vs), 1292 (s), 1062 (multiple, br), 771 (s) cm^{-1}. Absorption spectrum (MeCN), λ_{max}, cm^{-1}/nm (ϵ_M, L mol^{-1} cm^{-1}): 41 000/244 (5.4×10^4), 29 499/339 (1.7×10^4), 23 600/424-(1.4×10^4), 18 100/553 (9.9×10^2).

[(TPyA)Fe^{II}(CA^{2-})Fe^{II}(TPyA)](BF$_4$)$_2$·2MeOH (2^{2+}). A MeOH solution (20 mL) of $Fe(BF_4)_2$·$6H_2O$ (232 mg, 0.688 mmol) was added to a MeOH solution (10 mL) of TPyA (200 mg, 0.688 mmol) and a MeOH solution (10 mL) of chloranilic acid (H_2CA, 72 mg, 0.344 mmol) in a wet box (<1 ppm O_2), and the color became dark green and some dark solid formed. Triethylamine (0.10 mL, 0.688 mmol) was added for neutralization, and the solution turned yellow-brown and was heated to reflux for 30 min. The solution was allowed to stand at room temperature for 2 or 3 days, and dark green crystals formed that were collected by filtration, washed with methanol, and dried in vacuo to afford 235 mg (60%) of **2**$^{2+}$. Anal. Calcd for $C_{44}H_{44}B_2Cl_2F_8Fe_2N_8O_6$: C, 46.48; H, 3.90; N, 9.85. Found: C, 46.30; H, 3.81; N, 9.65. FT−IR (KBr): ν_{OH} 3429, ν_{CH} 3080, 2924, ν_{CN} 1607, ν_{CO} 1524, 1377, ν_{BF} 1060, 851, 767 cm^{-1}. Absorption spectrum (CH_2Cl_2), λ_{max}, cm^{-1}/nm (ϵ_M, L mol^{-1} cm^{-1}): 29 100/344 (1.0×10^4), 22 500/445 (sh, 3.3×10^3), 12 240/817 (sh, 2.6×10^3), 11 040/906 (2.7×10^3).

[(TPyA)Fe^{II}(CA$^{\bullet 3-}$)Fe^{II}(TPyA)](BF$_4$)·2Et$_2$O (2$^+$). To an MeCN solution (5 mL) of **2**$^{2+}$ (51 mg, 0.045 mmol) was added an MeCN solution (5 mL) of $CoCp_2$ (8.5 mg, 0.045 mmol) in a dry box (<1 ppm O_2). The color turned dark red-brown, and the solution was stirred for 1 h at room temperature. Red-brown needle-shaped crystals of **2**$^+$ were obtained by diffusion of diethyl ether into the reaction mixture of acetonitrile for 2 or 3 days, which were collected by filtration, washed with MeCN, and dried in vacuo (yield: 35 mg, 69%). Anal. Calcd for $C_{42}H_{36}BCl_2Fe_2F_4N_8O_4$: C, 51.15; H, 3.68; N, 11.36. Found: C, 50.89; H, 3.81; N, 11.31. FT−IR (KBr): ν_{CH} 3075 (w), 2925 (w), 1603 (s), 1572 (w), 1536 (w), ν_{CO} 1452 (vs), 1266 (w), 1051 (multiple, br), 832 (s), 765 (s) cm^{-1}. Absorption spectrum (MeCN), λ_{max}, cm^{-1}/nm (ϵ_M, L mol^{-1} cm^{-1}): 21 100/474(3.4×10^3), 18 300/546 (sh, 1.5×10^3). Attempts to obtain crystals suitable for single-crystal X-ray diffraction were unsuccessful, as only cottonlike crystals formed. Since the composition and IR spectrum of **2**$^+$ were the same as those of **1**$^+$, **2**$^+$ was assumed to be isostructural to **1**$^+$.

X-ray Crystallographic Data Collection and Refinement. Dark red crystals of **1**$^{3+}$, dark brown crystals of **1**$^{4+}$, and dark green crystals of **2**$^{2+}$ were mounted on a CryoLoop with Paratone oil. Intensity data for **1**$^{3+}$ were collected with an Enraf-Nonius KappaCCD diffractometer, and intensity data for **1**$^{4+}$ and **2**$^{2+}$ were collected with a Bruker SMART automatic diffractometer. For **1**$^{3+}$, the data were integrated and corrected for Lorentz and polarization effects using DENZO, and the scaling and the global refinement of crystal parameters were performed by SCALEPACK.[17] For **1**$^{4+}$ and **2**$^{2+}$, the data were integrated using the Bruker SAINT software program and scaled using the Bruker SADABS software program.[18] The crystal structures were solved by direct (**1**$^{3+}$, **2**$^{2+}$)[19] or Patterson methods (**1**$^{4+}$)[20] and refined by full-matrix least-squares methods using SHELXL-97.[21] The positions of all non-hydrogen atoms were refined with anisotropic displacement factors. All hydrogen atoms were placed using a riding model, and their positions were constrained relative to their parent atom using the appropriate HFIX command in SHELXL-97. Due to disorder, the four BF_4^- anions and one MeCN per unit cell of **1**$^{4+}$ and the diethyl ether for **2**$^{2+}$ were treated with the SQUEEZE routine in the program PLATON[22] and omitted from the final refinements, but are included in the computation of intensive properties. The crystallographic data of **1**$^{3+}$, **1**$^{4+}$, and **2**$^{2+}$ including **1**$^{2+}$ and **1**$^+$ are summarized in Table 1.

Results and Discussion

Using TPyA (tris(2-pyridylmethyl)amine) as an ancillary tetradentate capping ligand, dication dinuclear compounds of [(TPyA)M^{II}(CA^{2-})M^{II}(TPyA)]$^{2+}$ [M = Co (**1**$^{2+}$), Fe (**2**$^{2+}$)] composition were prepared.

Electrochemistry. The cyclic voltammetry (CV) of **1**$^{2+}$ in MeCN reveals four reversible one-electron transfer waves at $E_{1/2}$ = 0.619, 0.094, −0.619, and −1.388 V vs SCE (Figure 1). The former two processes correspond to two successive one-electron oxidations (**1**$^{3+}$/**1**$^{4+}$, **1**$^{2+}$/**1**$^{3+}$), and the latter, to two successive one-electron reductions (**1**$^{2+}$/**1**$^+$, **1**$^+$/**1**^{0}) of **1**$^{2+}$ as shown in Scheme 2. These potentials suggest that **1**$^{n+}$ (n = 1, 3, 4) can be isolated from reduction with $CoCp_2$ and oxidation with $Fc(BF_4)$ and $Thian(BF_4)$, respectively.

While the CVs for [(CTH)Co(DHBQ)Co(CTH)]$^{2+}$ and [(TPyA)Co(DHBQ)Co(TPyA)]$^{2+}$ were not reported,[8b,c] we prepared and determined that [(TPyA)Co^{II}(DHBQ^{2-})Co^{II}(TPyA)](BF$_4$)$_2$ in MeCN exhibits three reversible one-electron transfer waves at $E_{1/2}$ = 0.356, 0.086, and −0.866 V vs SCE. The mono-

(17) Otwinowski, Z.; Minor, W. Processing of X-ray Diffraction Data Collected in Oscillation Mode. *Methods Enzymol.* **1997**, *276*, 307.
(18) (a) *Saint Plus*, v. 6.02; Bruker Analytical X-ray: Madison, WI, 1999. (b) Sheldrick G. M. *SADABS*; University of Göttingen: Germany, 1996.
(19) (a) Altomare, A.; Burla, M. C.; Camalli, M.; Cascarano, G.; Giacovazzo, C.; Guagliardi, A.; Moliterni, A. G. G.; Polidori, G.; Spagna, R. *SIR97* (Release 1.02) - A program for automatic solution and refinement of crystal structure. (b) Burla, M. C.; Caliandro, R.; Camalli, M.; Carrozzini, B.; Cascarano, G. L.; De Caro, L.; Giacovazzo, C.; Polidori, G.; Spagna, R. *SIR2004*.
(20) Beurskens, P. T.; Beurskens, G.; de Gelder, R.; Garcia-Granda, S.; Gould, R. O.; Israel, R.; Smits, J. M. M. *The DIRDIF-99 program system*; Crystallography Laboratory, University of Nijmegen: The Netherlands, 1999.
(21) Sheldrick G. M. *SHELXL97, program for the crystal structure refinement*; University of Göttingen: Germany 1997.
(22) Spek, A. L. *J. Appl. Crystallogr.* **2003**, *36*, 7.

Table 1. Summary of the Crystallographic Data for $\mathbf{1}^{n+}$ (n = 1, 2, 3, 4) and $\mathbf{2}^{2+}$

	$\mathbf{1}^{2+}$	$\mathbf{1}^{+}$	$\mathbf{1}^{3+}$	$\mathbf{1}^{4+}$	$\mathbf{2}^{2+}$
formula	$C_{44}H_{44}B_2Cl_2Co_2F_8N_8O_6$	$C_{50}H_{56}BCl_2Co_2F_4N_8O_6$	$C_{50}H_{48}B_3Cl_2Co_2F_{12}N_{12}O_4$	$C_{44}H_{39}B_4Cl_2Co_2F_{16}N_9O_4$	$C_{44}H_{44}B_2Cl_2F_8Fe_2N_8O_6$
M_r	1143.25	1140.60	1330.19	1293.83	1137.10
crystal system	monoclinic	monoclinic	monoclinic	triclinic	monoclinic
space group	*C*2/*c*	*P*2/*n*	*C*2/*c*	$P\bar{1}$	*C*2/*c*
a (Å)	26.785(3)	13.846(7)	24.322(1)	9.005(2)	26.758(4)
b (Å)	10.884(1)	11.493(6)	15.584(1)	10.239(2)	10.976(2)
c (Å)	16.707(2)	15.958(8)	16.670(1)	14.930(4)	16.503(3)
α (deg)	90	90	90	88.531(4)	90
β (deg)	92.832(2)	90.687(9)	116.988(1)	79.184(4)	93.324(2)
γ (deg)	90	90	90	77.100(4)	90
V (Å^3)	4864.6(9)	2539(2)	5630.0(2)	1317.8(5)	4838.7(13)
Z	4	2	4	1	4
D_{calcd} (g cm^{-3})	1.561	1.492	1.569	1.630	1.561
T (K)	208(2)	208(2)	150(2)	208(2)	218(2)
λ (Å)	0.710 73	0.710 73	0.710 73	0.710 73	0.710 73
μ (mm^{-1})	0.879	0.831	0.780	0.840	0.797
R_1[a] (4σ data)	0.0545	0.0469	0.0436	0.0641	0.0464
wR_2[b] (4σ data)	0.1399	0.1300	0.0946	0.1465	0.1161

[a] $R_1 = \Sigma||F_o| - |F_c||/\Sigma|F_o|$. [b] $wR_2 = [\Sigma w(F_o^2 - F_c^2)^2/\Sigma w(F_o^2)^2]^{1/2}$.

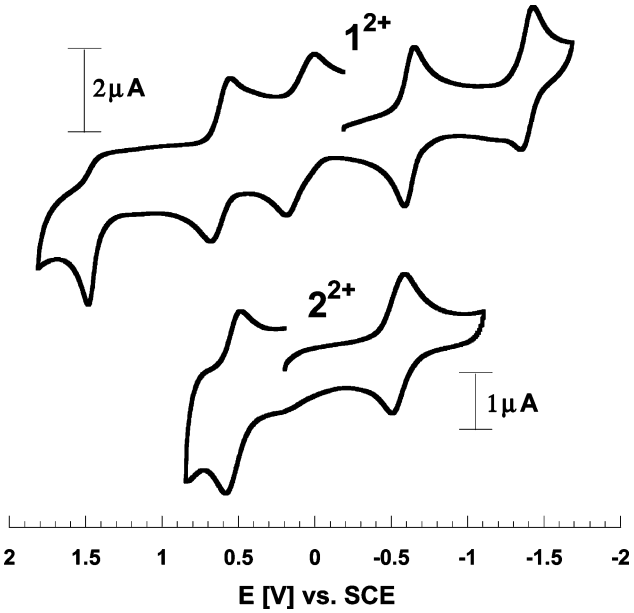

Figure 1. Cyclic voltammetry of $\mathbf{1}^{2+}$ (top) and $\mathbf{2}^{2+}$ (bottom) at 20 °C in MeCN and CH_2Cl_2 solutions, respectively [0.1 M [(*n*-Bu)$_4$N]BF_4 supporting electrolyte; platinum working electrode; scan rate 100 mV/s, ferrocene internal standard].

oxidation potential of $\mathbf{1}^{2+}$ (0.094 V) is similar to that of [(TPyA)Co^{II}(DHBQ^{2-})Co^{II}(TPyA)]$^{2+}$ (0.086 V); however, the second oxidation and monoreduction potentials of $\mathbf{1}^{2+}$ (0.619 and −0.619 V) are higher than those of [(TPyA)Co^{II}(DHBQ^{2-})-Co^{II}(TPyA)]$^{2+}$ (0.356 and −0.866 V), respectively. Hence, the monoreduction of $\mathbf{1}^{2+}$ and dioxidation of [(TPyA)Co^{II}(DHBQ^{2-})-Co^{II}(TPyA)]$^{2+}$ occur more easily.

The CV of $\mathbf{2}^{2+}$ shows a reversible one-electron oxidation ($\mathbf{2}^{2+}$/$\mathbf{2}^{3+}$) at 0.535 V and a reversible one-electron reduction ($\mathbf{2}^{2+}$/$\mathbf{2}^{+}$) at −0.547 V (Figure 1) that correspond to ligand- and/or metal-centered processes. These potentials suggest that $\mathbf{2}^{n+}$ (n = 1, 3) can be isolated from chemical reduction/oxidation with $CoCp_2$ and Thian(BF_4), respectively.

The CV of [(CTH)Fe(DHBQ)Fe(CTH)]$^{2+}$ in MeCN showed three well-separated reversible one-electron transfer waves at $E_{1/2}$ = 0.769, 0.199, and −0.891 V vs SCE.[8a] Thus, the one-electron oxidation (2+/3+) of $\mathbf{2}^{2+}$ is 0.336 V higher and thus harder to oxidize, as observed. However, the one-electron reduction (+/2+) of $\mathbf{2}^{2+}$ is −0.547 V and is 0.344 V higher than that for [(CTH)Fe(DHBQ)Fe(CTH)]$^{2+}$ and is easier to reduce, as occurred.

Scheme 2

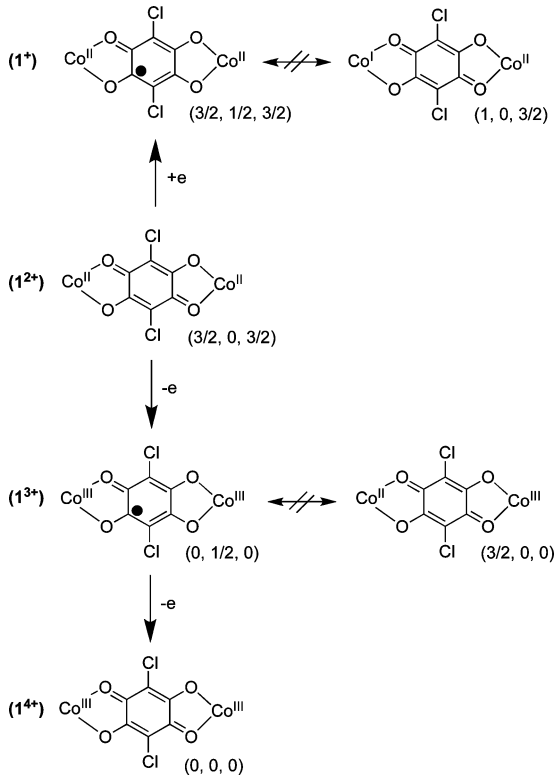

Synthesis and Characterization. In accord with the CV, $\mathbf{1}^{3+}$ and $\mathbf{1}^{4+}$ were respectively prepared from the oxidation with 1 equiv of Fc(BF_4) and 2 equiv of thianthrinium tetrafluoroborate (Thian$^+$/Thian, 1.23 V vs SCE)[23] at room temperature in a dry box, respectively. Dark red and dark brown crystals of valence ambiguous [(TPyA)Co(CA)Co(TPyA)](BF_4)$_3$·4MeCN ($\mathbf{1}^{3+}$) and fully oxidized [(TPyA)Co^{III}(CA^{2-})Co^{III}(TPyA)](BF_4)$_4$·MeCN ($\mathbf{1}^{4+}$) were obtained in 71% and 81% yields, respectively. Reductions of $\mathbf{1}^{2+}$ to $\mathbf{1}^{+}$ and $\mathbf{2}^{2+}$ to $\mathbf{2}^{+}$ were achieved from the

(23) Connelly, N. G.; Geiger, W. E. *Chem. Rev.* **1996**, *96*, 877.

Table 2. Selected Bond Distances, Å, for $\mathbf{1}^{n+}$ (n = 1, 2, 3, 4) and $\mathbf{2}^{2+}$

	$\mathbf{1}^{2+a}$	$\mathbf{1}^{+a}$	$\mathbf{1}^{3+}$	$\mathbf{1}^{4+}$	$\mathbf{2}^{2+}$
M−N1	2.110(3)	2.085(2)	1.919(2)	1.912(3)	2.125(2)
M−N2	2.239(3)	2.262(2)	1.933(2)	1.906(3)	2.291(2)
M−N3	2.080(3)	2.090(2)	1.917(2)	1.912(3)	2.153(2)
M−N4	2.108(3)	2.109(2)	1.899(2)	1.879(3)	2.169(2)
M−O1	2.030(2)	1.978(2)	1.885(2)	1.878(2)	2.063(2)
M−O2	2.277(3)	2.166(2)	1.896(2)	1.904(2)	2.212(2)
M−L_{av}	2.122(1)	2.115(1)	1.908(1)	1.896(1)	2.169(1)
C19−O1	1.266(4)	1.304(3)	1.316(3)	1.275(4)	1.270(3)
C20−O2	1.246(4)	1.282(2)	1.307(3)	1.252(4)	1.251(3)
C19−C20	1.527(5)	1.473(3)	1.456(3)	1.507(4)	1.528(3)
C19−C21	1.372(5)	1.386(3)	1.386(3)	1.365(4)	1.382(3)
C20−C21a	1.409(5)	1.400(3)	1.395(3)	1.374(4)	1.405(3)
C21−Cl1	1.729(4)	1.743(2)	1.723(2)	1.701(3)	1.732(2)

[a] Reference 12.

reaction of 1 equiv of cobaltocene ($CoCp_2/CoCp_2^+$, −0.91 V vs SCE[23]) at room temperature in a dry box. Dark red-brown very air-sensitive crystals of $[(TPyA)Fe^{II}(CA^{\bullet 3-})Fe^{II}(TPyA)](BF_4)\cdot 2Et_2O$ ($\mathbf{2}^+$) were obtained in 69% yield. Attempts to obtain valence ambiguous $[(TPyA)Fe(CA)Fe(TPyA)](BF_4)_3$ ($\mathbf{2}^{3+}$) from $\mathbf{2}^{2+}$ failed due to the decomposition of the dimer during the oxidation process. This is not surprising due to the higher potential needed for $\mathbf{2}^{3+}$ with respect to $\mathbf{1}^{3+}$. The structures and electronic structures of $\mathbf{1}^{n+}$ (n = 1, 2, 3, 4) and $\mathbf{2}^{n+}$ (n = 1, 2), and particularly that of valence ambiguous $\mathbf{1}^{3+}$, were elucidated from the elemental analysis, infrared spectrum, UV/vis spectrum, electrochemistry, solution EPR, solid-state magnetochemistry, and single-crystal X-ray diffraction analysis.

Structures. The crystal structures of dinuclear complexes [$\mathbf{1}^{n+}$ (n = 1, 2, 3, 4), $\mathbf{2}^{2+}$] were determined by X-ray crystallography at low temperature, their crystallographic data are summarized in Table 1, and selected bond distances are listed in Table 2. All complexes contain isostructural dimeric $[(TPyA)M(CA)M(TPyA)]^{n+}$ (M = Co, Fe; n = 1, 2, 3, 4) cations with a tetradentate TPyA ligand. The representative ORTEP structure of the $\mathbf{1}^{3+}$ cation is shown in Figure 2. The cations in the crystal structures of $\mathbf{1}^{4+}$ and $\mathbf{2}^{2+}$, including $\mathbf{1}^{2+}$ and $\mathbf{1}^+$, are very similar and are not shown (see Supporting Information), and all cations have the identical atom labeling for easy comparison in Table 2. The oxidation states of the M as well as CA^{n-} were identified from the observed bond distances and verified from magnetic and spectroscopic studies.

$\mathbf{1}^{2+}\cdot$2MeOH. The average Co−N_{TPyA} and Co−$O_{chloranilate}$ bond distances are 2.134(2) and 2.106(2) Å, respectively, and are characteristic of Co(II) (vide infra).[24] The C19−C20 and average C−O chloranilate bond distances are 1.527(5) and 1.256(3) Å, respectively, and are characteristic of CA^{2-} (vide infra).[25] The average bite distance of the chloranilate five-member chelate ring is 2.608(4) Å. The cobalt(II) ion is 0.322(5) Å out of the chloranilate-coordination plane. The shortest intradimer Co···Co separation is 8.090(1) Å, and it is 9% longer than the shortest interdimer Co···Co separation of 6.791(1) Å.

The pyridyl groups of $\mathbf{1}^{2+}$ are involved in extensive $\pi-\pi$ stacking interactions, with C−H···π interactions and offset face-to-face $\pi-\pi$ interactions (Figure 3a).[26] Between the dimers, the two pyridine rings involving N3 and N2 ($-x+1, -y, -z+1$) are $\pi-\pi$ stacked with the herringbone structure: H···centroid, 2.88 Å; ∠C−H-centroid, 136.1°; centroid···centroid, 4.82 Å; dihedral angle between two pyridine rings, 82.3°. Additionally, the pyridine group involving N3 located in a dimer undergoes the offset $\pi-\pi$ interaction with the pyridine group involving N3 ($-x+1, -y, -z+1$), which is positioned at the neighboring dimer. The interplanar separation of the pyridine rings is ~3.65 Å (centroid···centroid, 4.11 Å), and the dihedral angle and the offset angle between the pyridine ring planes are 0.0° and 6.3°, respectively. Due to these interdimer offset face-to-face $\pi-\pi$ and herringbone interactions, $\mathbf{1}^{2+}$ forms a 1-D polymeric chain (Figure 3a).

$\mathbf{1}^{+}\cdot 2Et_2O$. The average Co−$N_{TPyA}$ and Co−$O_{chloranilate}$ bond distances are 2.137(1) and 2.072(1) Å, respectively. These values are similar to those of $\mathbf{1}^{2+}$, indicating that the oxidation state of cobalt ion in $\mathbf{1}^+$ is same as that of $\mathbf{1}^{2+}$. The C19−C20 and average C−O chloranilate bond distances are 1.473(3) and 1.289(2) Å, respectively. These bond distances significantly differ from those for $\mathbf{1}^{2+}$ by −0.054 to 0.033 Å, respectively. The differences are attributed to the ligand-centered reduction of CA^{2-} to $CA^{\bullet 3-}$ and population of the antibonding orbital and are in accord with the Co−N_{TPyA} and Co−$O_{chloranilate}$ distances without the reduction of Co(II). The average bite distance of the chloranilate five-member chelate ring is 2.657(3) Å. The cobalt(II) ion is 0.101(4) Å out of the chloranilate-coordination plane. The shortest intradimer Co···Co separation is 7.926(1) Å and is a bit longer (1%) than the shortest interdimer Co···Co distance of 7.856(1) Å.

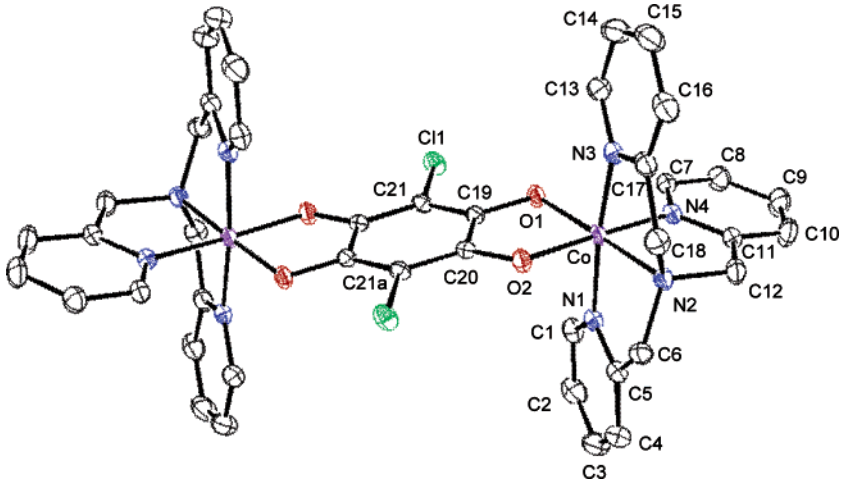

Figure 2. Structure of the $[(TPyA)Co^{III}(CA^{\bullet 3-})Co^{III}(TPyA)]^{3+}$ ($\mathbf{1}^{3+}$). The atoms are represented by 40% probable thermal ellipsoids. This atom labeling diagram of the cations is the same for $\mathbf{1}^{n+}$ (n = 1, 2, 3, 4) and $\mathbf{2}^{2+}$. H atoms, solvent, and $[BF_4]^-$ are omitted for clarity.

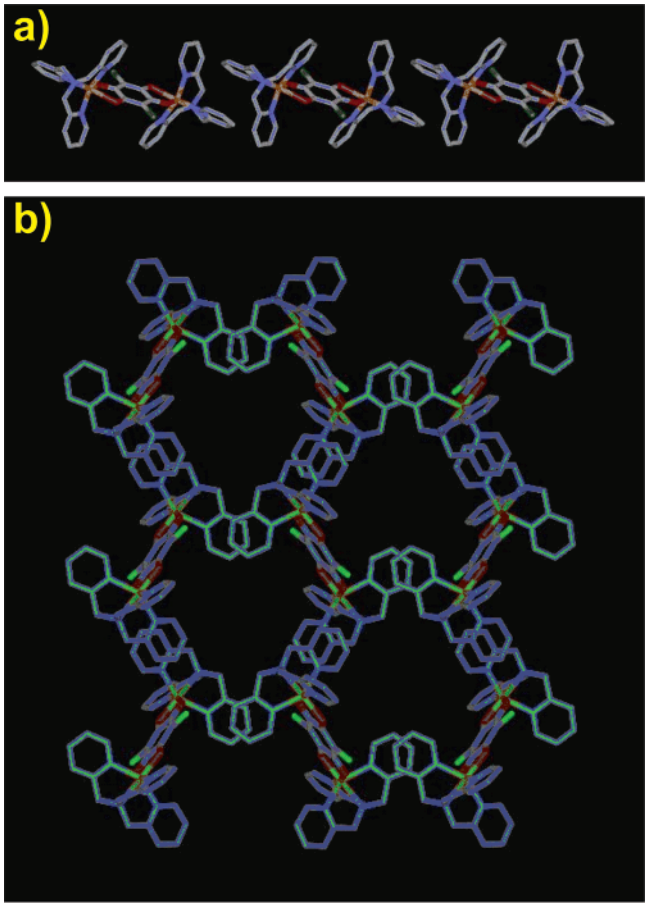

Figure 3. (a) Perspective view of $\mathbf{1}^{2+}$ showing a 1-D polymer by C−H···π interactions and offset face-to-face $\pi-\pi$ interactions. The structure of $\mathbf{2}^{2+}$ is isomorphous to $\mathbf{1}^{2+}$. (b) Extended 2-D structure of $\mathbf{1}^{+}$ by offset face-to-face $\pi-\pi$ interaction.

$\mathbf{1}^{+}$ has extensive offset face-to-face $\pi-\pi$ interactions between the pyridyl groups (Figure 3b).[26] Between the dimers the two pyridine rings involving N1 and N3 are $\pi-\pi$ stacked with the offset face-to-face $\pi-\pi$ interactions. The pyridine group involving N1 and N3 located in a dimer undergo the offset $\pi-\pi$ interaction with the pyridine group involving N1 ($-x$, $-y$, $-z+1$) and N3 ($-x+0.5$, y, $-z+1.5$), which belong to different dimers, respectively. The interplanar separations of the pyridine rings are ~3.39 Å (centroid···centroid, 3.62 Å) and 3.29 to 3.43 Å (centroid···centroid, 3.54 Å), respectively, and the dihedral angles between the pyridine ring planes are 0.0° and 2.8°, respectively. Due to these interdimer offset face-to-face $\pi-\pi$ interactions, $\mathbf{1}^{+}$ has a 2-D layer square motif (Figure 3b).

$\mathbf{1}^{3+}$•4MeCN. The average Co−N_{TPyA} and Co−$O_{chloranilate}$ bond distances are 1.917(1) and 1.891(1) Å, respectively. The chloranilate C19−C20 and average C−O bond distances are 1.456(3) and 1.312(2) Å, respectively. These distances are close to those of chloranilate in $\mathbf{1}^{+}$, indicative of $CA^{\bullet 3-}$. The average bite distance of the chloranilate five-member chelate ring is 2.606(4) Å. The cobalt(III) ion is 0.282(7) Å out of the chloranilate-coordination plane. The shortest intradimer Co···Co separation is 7.470(1) Å and is 14% less than the shortest interdimer Co···Co distance of 8.719(1) Å.

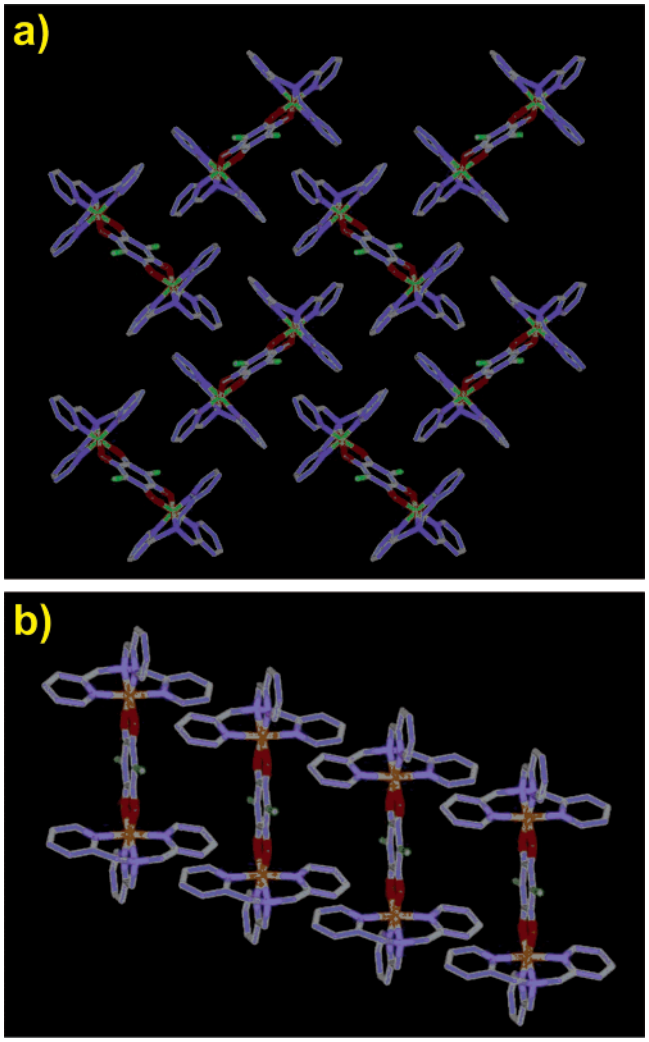

Figure 4. (a) Extended 2-D structure of $\mathbf{1}^{3+}$ by C−H···π interactions and offset face-to-face $\pi-\pi$ interactions. (b) Perspective view of $\mathbf{1}^{4+}$ showing a ladderlike 1-D polymer by offset face-to-face $\pi-\pi$ interactions.

The chloranilate group is involved in C−H···π interactions (Figure 4a).[26] Between the dimers, the chloranilate and the pyridine rings involving N1 ($-x+0.5$, $y+0.5$, $-z+0.5$) are $\pi-\pi$ stacked with the herringbone structure: H···centroid, 2.98 Å; ∠C−H−centroid, 135.9°; centroid···centroid, 4.90 Å; dihedral angle between two pyridine rings, 88.7°. Additionally, the pyridine groups involving N2 and N3 ($-x+0.5$, $-y+0.5$, $-z$) located in a dimer undergo the offset $\pi-\pi$ interaction with the pyridine group involving N1 ($-x+0.5$, $y+0.5$, $-z+0.5$), which is positioned at the neighboring dimer. The centroid separations between the pyridine rings are 4.18 and 4.89 Å, respectively, and the dihedral angles between the pyridine ring planes are 32.7° and 27.1°, respectively. Due to these interdimer offset face-to-face $\pi-\pi$ and herringbone interactions, $\mathbf{1}^{3+}$ has a 2-D sheet motif (Figure 4a).

$\mathbf{1}^{4+}$•MeCN. The average Co−N_{TPyA} and Co−$O_{chloranilate}$ bond distances are 1.902(2) and 1.891(1) Å, respectively. The chloranilate C19−C20 and average C−O bond distances are 1.507(4) and 1.264(3) Å, respectively. These distances are very similar to those of chloranilate in $\mathbf{1}^{2+}$, indicative of CA^{2-}. The

(24) (a) Xie, Y.-B.; Li, J.-R.; Zhang, C.; Bu, X.-H. *Cryst. Growth Des.* **2005**, *5*, 1743. (b) Hossain, M. J.; Yamasaki, M.; Mikuriya, M.; Kuribayashi, A.; Sakiyama, H. *Inorg. Chem.* **2002**, *41*, 4058.
(25) (a) Kennedy, A. R.; Waterson, F. R. N. *Acta Crystallogr.* **2003**, *C59*, o613. (b) Ishida, H.; Kashino, S. *Acta Crystallogr.* **2001**, *C57*, 476.
(26) (a) Desiraju, G. R. *Crystal Engineering: The Design of Organic Solids*; Elsevier: New York, 1989; Chapter 4. (b) Shetty, A. S.; Zhang, J.; Moore, J. S. *J. Am. Chem. Soc.* **1996**, *118*, 1019. (c) Jennings, W. B.; Farrell, B. M.; Malone, J. F. *Acc. Chem. Rev.* **2001**, *34*, 885.

average bite distance of the chloranilate five-member chelate ring is 2.546(4) Å. The cobalt(III) ion is 0.094(13) Å out of the chloranilate-coordination plane. The shortest intradimer Co···Co separation is 7.454(1) Å and is 17% less than the shortest interdimer Co···Co distance of 9.005(1) Å.

The packing structure displays extensive $\pi-\pi$ stacking interactions, such as offset face-to-face $\pi-\pi$ interactions, between the pyridyl groups (Figure 4b).[26] The pyridine group involving N1 located in a dimer undergoes the offset $\pi-\pi$ interaction with the pyridine group involving N3 ($x-1, y, z$), which is positioned at the neighboring dimer. The interplanar separation of the pyridine rings is 3.42 to 3.66 Å (centroid···centroid, 4.22 Å), and the dihedral angle between the pyridine ring planes is 5.8°. Due to these interdimer offset, face-to-face $\pi-\pi$ interactions, $\mathbf{1}^{4+}$ has a 1-D ladderlike chain structure (Figure 4b).

$\mathbf{2}^{2+}$·2MeOH. The average Fe−N_{TPyA} and Fe−$O_{chloranilate}$ bond distances are 2.185(1) and 2.133(1) Å, respectively. The chloranilate C19−C20 and average C−O bond distances are 1.528(3) and 1.261(2) Å, respectively. These values are similar to those of chloranilate in $\mathbf{1}^{2+}$ and $\mathbf{4}^{+}$, indicating CA^{2-}, not $CA^{\bullet 3-}$, is present. The average bite distance of the chloranilate five-member chelate ring is 2.609(2) Å. The iron(II) ion is 0.291(3) Å out of the chloranilate-coordination plane. The shortest Fe···Fe intradimer separation within the dimer is 8.063(1) Å and is 20% greater than the shortest interdimer Fe···Fe distance of 6.734(1) Å.

As is observed for $\mathbf{1}^{2+}$, the pyridyl groups display extensive $\pi-\pi$ stacking interactions, such as C−H···π interactions and offset face-to-face $\pi-\pi$ interactions (see Figure 3a).[26] Between the dimers, the two pyridine rings involving N4 and N3 ($-x+1, -y+1, -z$) are $\pi-\pi$ stacked with the herringbone structure: H···centroid, 2.86 Å; ∠C−H−centroid, 134.9°; centroid···centroid, 4.79 Å; dihedral angle between two pyridine rings, 85.0°. Furthermore, the pyridine group involving N3 located in a dimer undergoes the offset $\pi-\pi$ interaction with the pyridine group involving N3 ($-x+1, -y+1, -z$) belonging to the neighboring dimer. The interplanar separation of the pyridine rings is ~3.53 Å (centroid···centroid, 3.98 Å), and the dihedral angle and the offset angle between the pyridine ring planes are 0.0° and 26.8°, respectively. Due to these interdimer offset face-to-face $\pi-\pi$ and herringbone interactions, $\mathbf{2}^{2+}$ forms a 1-D polymeric chain.

Electronic Structure Assignment and Summary of the Structural Data. All of the M−N and M−O bond distances for $\mathbf{1}^{2+}$ and $\mathbf{1}^{+}$ are typical for octahedral cobalt(II) ions (d^7, $S = {}^3/_2$), while those for $\mathbf{1}^{3+}$ and $\mathbf{1}^{4+}$ are typical for low-spin cobalt(III) (d^6, $S = 0$), and those for $\mathbf{2}^{2+}$ are typical for the high-spin iron(II) ion (d^6, $S = 2$).[27] The average chloranilate C(19)−O(1) and C(20)−O(2) bond distances of 1.289(2) and 1.312(2) Å in $\mathbf{1}^{+}$ and $\mathbf{1}^{3+}$ are longer than the 1.256(3) to 1.264(3) Å of $\mathbf{1}^{2+}$, $\mathbf{1}^{4+}$, and $\mathbf{2}^{2+}$, while the 1.456(3)−1.473(3) Å C(19)−C(20) distances in $\mathbf{1}^{+}$ and $\mathbf{1}^{3+}$ are shorter than the 1.507(4) to 1.528(3) Å for $\mathbf{1}^{2+}$, $\mathbf{1}^{4+}$, and $\mathbf{2}^{2+}$. This indicates that $CA^{\bullet 3-}$ is present in $\mathbf{1}^{+}$ and $\mathbf{1}^{3+}$, while $\mathbf{1}^{2+}$, $\mathbf{1}^{4+}$, and $\mathbf{2}^{2+}$ possess CA^{2-}. Thus, the structures clearly demonstrate the oxidation and electronic states of the metal ions and the presence of CA^{2-} and $CA^{\bullet 3-}$ in the complexes, i.e., Co(II)(*hs*)−L_{av} = 2.115(1)−2.122(1) Å, Co(III)(*ls*)−L_{av} = 1.896(1)−1.908(1) Å, and Fe(II)(*hs*)−L_{av} = 2.169(1) Å. Additionally, the average bite angles of five-member chelate rings involving in TPyA and chloranilate are 74.25(12)° to 79.64(10)° for $\mathbf{1}^{2+}$, $\mathbf{1}^{+}$, and $\mathbf{2}^{2+}$ and 84.64(9)° to 87.15(7)° for $\mathbf{1}^{3+}$ and $\mathbf{1}^{4+}$. The former is smaller than the latter, due to the difference of ionic radii in different oxidation states, i.e., Co^{2+}(0.885 Å)/Fe^{2+}(0.920 Å) and Co^{3+}(0.58 Å).[28]

The average bite distances of the chloranilate five-member chelate ring for $\mathbf{1}^{2+}$, $\mathbf{1}^{+}$, $\mathbf{1}^{3+}$, $\mathbf{1}^{4+}$, and $\mathbf{2}^{2+}$ are 2.608(4), 2.657(3), 2.606(4), 2.546(4), and 2.609(2) Å, respectively, which are shorter than the bite distance of the noncoordinated oxygens of chloranilate, 2.688(3) Å, and also depend on the oxidation states of the metal ion and chloranilate. The distance of $\mathbf{1}^{2+}$ [2.608(4) Å] is shorter than that of $\mathbf{1}^{+}$ [2.657(3) Å], even though each cobalt ion has the same oxidation state. This one is attributed to the different oxidation states of chloranilate, i.e., CA^{2-} and $CA^{\bullet 3-}$. The distance of $\mathbf{1}^{4+}$ [2.546(4) Å] is also shorter than that for $\mathbf{1}^{3+}$ [2.606(4) Å]. In the case of $\mathbf{2}^{2+}$, the bite distance [2.609(2) Å] is nearly the same as that of $\mathbf{1}^{2+}$, because the oxidation states of the metal ion and chloranilate are the same as those of $\mathbf{1}^{2+}$. The central cobalt and iron ions have small deviations [0.094(13) to 0.322(5) Å] out of the chloranilate-coordination plane, which is similar with respect to related compounds, and is indicative of the distortion of octahedral geometry in the complexes. Thus, from the structural data $\mathbf{1}^{2+}$, $\mathbf{1}^{+}$, $\mathbf{1}^{3+}$, $\mathbf{1}^{4+}$, and $\mathbf{2}^{2+}$ are formulated as having $[Co^{II}CA^{2-}Co^{II}]^{2+}$, $[Co^{II}CA^{\bullet 3-}Co^{II}]^{+}$, $[Co^{III}CA^{\bullet 3-}Co^{III}]^{3+}$, $[Co^{III}CA^{2-}Co^{III}]^{4+}$, and $[Fe^{II}CA^{2-}Fe^{II}]^{2+}$ cores, respectively, with $CA^{\bullet 3-}$ being present for $\mathbf{1}^{+}$ and $\mathbf{1}^{3+}$ and additionally $\mathbf{2}^{+}$.

Complex Induced Electron Transfer. Formation of the CA^{2-}-reduced, $CA^{\bullet 3-}$ related species $\mathbf{1}^{3+}$ as well as $[(CTH)Fe^{III}(DHBQ^{\bullet 3-})Fe^{III}(CTH)]^{3+}$, $[(CTH)Co(DHBQ^{\bullet 3-})Co(CTH)]^{3+}$, and $[(TPyA)Co(DHBQ^{\bullet 3-})Co(TPyA)]^{3+}$ [8] occurs via a complex electron-transfer reaction involving addition of an oxidant, not a reductant. This redox reaction is best described as a redox-induced electron rearrangement (RIER) whereby the one-electron oxidation of the $[M^{II}CA^{2-}M^{II}]^{2+}$ (M = Fe, Co) core forms $[M^{III}CA^{\bullet 3-}M^{III}]^{3+}$, not the expected mixed valent $[M^{II}CA^{2-}M^{III}]^{3+}$ core. Presumably, oxidation forms $[M^{II}CA^{2-}M^{III}]^{3+}$ that immediately undergoes an electron rearrangement, or isomerization (so-called valence tautomerization[9]), forming the observed $[M^{III}CA^{\bullet 3-}M^{III}]^{3+}$ species. Since mixed valent complexes [localized (Class I) or delocalized (Class III)] are relatively common and stable,[29] it is surprising that an electron rearrangement occurs for this valence ambiguous species.

EPR of $\mathbf{1}^{3+}$. The room-temperature X-band EPR spectrum of $\mathbf{1}^{3+}$ in MeCN consists of a 15-line pattern (Figure 5), as expected in a dinuclear cobalt(III) complex, and confirms the $S = {}^1/_2$ ground state of the trication $[(TPyA)Co^{III}(CA^{\bullet 3-})Co^{III}(TPyA)]^{3+}$. The spectrum was simulated with $g = 2.0027$, $A(^{59}Co) = 4.94$ G, and peak-to-peak line width = 2.5 G (Figure

(27) (a) Wang, H.; Liu, Z.; Liu, C.; Zhang, D.; Lu, Z.; Geng, H.; Shuai, Z.; Zhu, D. *Inorg. Chem.* **2004**, *43*, 4091. (b) Konar, S.; Zangrando, E.; Drew, M. G. B.; Mallah, T.; Ribas, J.; Chaudhuri, N. R. *Inorg. Chem.* **2003**, *42*, 5966. (c) Min, K. S.; Weyhermüller, T.; Wieghardt, K. *Dalton Trans.* **2003**, 1126.

(28) (a) Shannon, R. D.; Prewitt, C. T. *Acta Crystallogr.* **1970**, *B26*, 1046. (b) Yakel, H. L., Jr. *Acta Crystallogr.* **1955**, *8*, 394.

(29) (a) Demadis, K. D.; Hartshorn, C. M.; Meyer, T. J. *Chem. Rev.* **2001**, *101*, 2655. (b) D'Alessandro, D. M.; Topley, A. C.; Davies, M. S.; Keene, F. R. *Chem.—Eur. J.* **2006**, *12*, 4873. (c) Robin, M. B.; Day, P. *Adv. Inorg. Radiochem.* **1967**, *10*, 247. (d) Hush, N. *Progr. Inorg. Chem.* **1967**, *8*, 357.

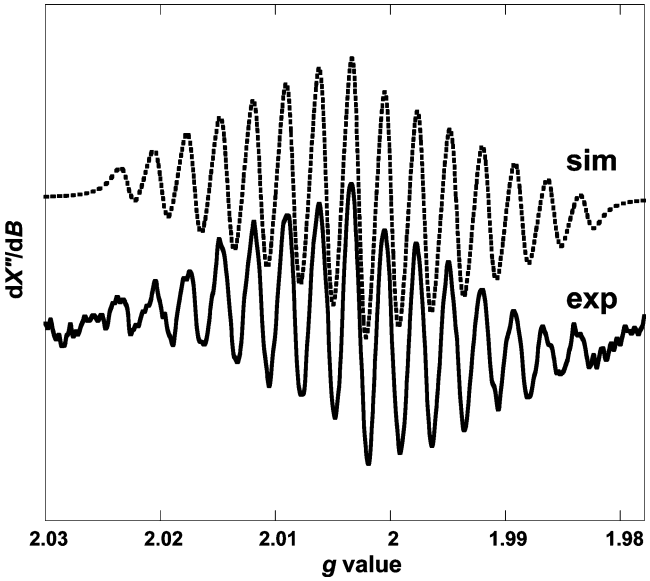

Figure 5. Simulated (sim; $g = 2.0027$, $A(^{59}\text{Co}) = 4.94$ G, and peak-to-peak line width = 2.5 G) and observed X-band EPR spectrum of $\mathbf{1}^{3+}$ (in MeCN, room temperature, 9.746 GHz, modulation amplitude 0.20 G, and 50 mW).

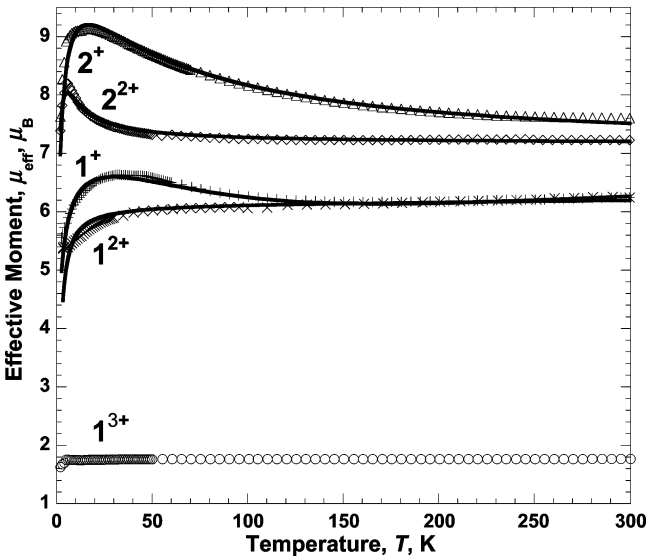

Figure 6. $\mu_{\text{eff}}(T)$ for $\mathbf{1}^{n+}$ [$n = 1$ (+), 2 (×), 3 (○)] and $\mathbf{2}^{n+}$ [$n = 1$ (△), 2 (◇)]. The solid lines are the best-fit curves to eqs 1−3, as discussed in the text.

5). If $S = {}^3/_2$ Co(II) was present, a signal should occur at $g \approx 4.3$. The observed ^{59}Co hyperfine coupling is very similar to data reported for a phenoxyl-Co(III) complex [$A(^{59}\text{Co}) = 6.0$ G)][30] and a small value compared to the coupling constants found for Co$^{\text{III}}$(benzosemiquinonate) [$A(^{59}\text{Co}) = 9.76$ to 20 G] and Co$^{\text{III}}$(iminobenzosemiquinonate) complexes [$A(^{59}\text{Co}) = 14$ G].[27c,31] Hence, the formulation of $\mathbf{1}^{3+}$ as [(TPyA)Co$^{\text{III}}$(CA$^{\bullet 3-}$)-Co$^{\text{III}}$(TPyA)]$^{3+}$ in the solid state is also the same in solution.

Magnetic Properties. The magnetic susceptibilities, χ, of $\mathbf{1}^{n+}$ ($n = 1, 2, 3, 4$) and $\mathbf{2}^{n+}$ ($n = 1, 2$) were measured between 2 and 300 K and are reported as $\mu_{\text{eff}}(T)$ [$= (8\chi T)^{1/2}$], Figure 6. $\mathbf{1}^{4+}$ is diamagnetic between 2 and 300 K. As reported earlier,[12] $\mathbf{1}^{2+}$ and $\mathbf{1}^{+}$ have room-temperature moments of 6.26 and 6.20 μ_{B}/Co$_2$ in accord with the moments of dinuclear complexes containing high-spin Co(II) that has a spin−orbit contribution.[32] The $\mu_{\text{eff}}(T)$ for $\mathbf{1}^{2+}$ and $\mathbf{1}^{+}$ were fit to analytical expressions, for a coupled $S = {}^3/_2$ dimer, eq 1 ($H = -2J\mathbf{S}_1\cdot\mathbf{S}_2$) and $F_i = F_1$, and for a linear three-spin system with $S_1 = S_3 = {}^3/_2$ and $S_2 = {}^1/_2$, eq 1 [$H = -2J(\mathbf{S}_1\cdot\mathbf{S}_2 + \mathbf{S}_2\cdot\mathbf{S}_3)$] and $F_i = F_2$.

$$\chi = [Ng^2\mu_{\text{B}}{}^2/k_{\text{B}}(T-\theta)]\,F_i(T) + \text{TIP} \qquad (1)$$

$$F_1(T) = [2\exp(2J/k_{\text{B}}T) + 10\exp(6J/k_{\text{B}}T) + 28\exp(12J/k_{\text{B}}T)]/[1 + 3\exp(2J/k_{\text{B}}T) + 5\exp(6J/k_{\text{B}}T) + 7\exp(12J/k_{\text{B}}T)]$$

$$F_2(T) = [84 + 35\exp(-J/k_{\text{B}}T) + 10\exp(-2J/k_{\text{B}}T) + \exp(-3J/k_{\text{B}}T) + \exp(-5J/k_{\text{B}}T) + 10\exp(-6J/k_{\text{B}}T) + 35\exp(-7J/k_{\text{B}}T)]/[16 + 12\exp(-J/k_{\text{B}}T) + 8\exp(-2J/k_{\text{B}}T) + 4\exp(-3J/k_{\text{B}}T) + 4\exp(-5J/k_{\text{B}}T) + 8\exp(-6J/k_{\text{B}}T) + 12\exp(-7J/k_{\text{B}}T)]$$

The best fit for $\mathbf{1}^{2+}$ is $J/k_{\text{B}} = -0.65$ K (-0.45 cm^{-1}), $g = 2.24$, $\theta = -0.1$ K, and TIP = 400×10^{-6} emu/mol, and that for $\mathbf{1}^{+}$ is J/k_{B} of -75 K (-52 cm^{-1}), $g = 2.36$, $\theta = -2.6$ K, and TIP = 400×10^{-6} emu/mol. While both exhibit antiferromagnetic coupling, the magnitude of J for $\mathbf{1}^{+}$ is 2 orders larger than that for $\mathbf{1}^{2+}$. This is attributed to the presence of direct exchange coupling arising from the overlap of the π^* SOMO of $S = {}^1/_2$ CA$^{\bullet 3-}$ and t_{2g} orbitals of $S = {}^3/_2$ Co(II) ion that is not present for $\mathbf{1}^{2+}$, in which the weaker spin coupling occurs via superexchange.[13] It should be noted that the increase in $\mu_{\text{eff}}(T)$ with decreasing temperature below 120 K for $\mathbf{1}^{+}$ is suggestive of ferromagnetic coupling. However, as modeled, this is solely due to antiferromagnetic coupling, and several other examples where antiferromagnetic coupling leads to an increase in $\mu_{\text{eff}}(T)$ with decreasing temperature have been reported.[33]

The $\mu_{\text{eff}}(T)$ of $\mathbf{1}^{3+}$ is temperature independent and has a room-temperature moment of 1.75(2) μ_{B} consistent with $S = {}^1/_2$ CA$^{\bullet 3-}$ ($\chi_{\text{TIP}} = 40 \times 10^{-6}$ emu mol^{-1}, $g = 2.0$, $\theta = -0.62$ K) and a diamagnetic cobalt(III) ion (d^6, $S_{\text{Co}} = 0$), which typically has a TIP of 55 to 200 $\times 10^{-6}$ emu mol^{-1},[27c,34] in accord with the EPR spectrum. In contrast to [(CTH)Co(DHBQ$^{\bullet 3-}$)Co(CTH)]$^{3+}$ [8b] and [(TPyA)Co(DHBQ$^{\bullet 3-}$)Co(TPyA)]$^{3+}$ [8c] which undergo Co$^{\text{III}}$(DHBQ$^{\bullet 3-}$)Co$^{\text{III}}$ ↔ Co$^{\text{II}}$(DHBQ^{2-})Co$^{\text{III}}$ spin crossover, $\mathbf{1}^{3+}$ does not exhibit spin crossover below 375 K. This behavior is attributed to the electron withdrawing Cl group, which stabilizes trianionic CA$^{\bullet 3-}$ favoring the left-hand side of [Co$^{\text{III}}$CA$^{\bullet 3-}$Co$^{\text{III}}$]$^{3+}$ ↔ [Co$^{\text{II}}$CA^{2-}Co$^{\text{III}}$]$^{3+}$.

The 7.23 μ_{B} room-temperature moment for $\mathbf{2}^{2+}$ is nearly constant with decreasing temperature until 50 K (Figure 6). This value is slightly larger than the value (6.93 μ_{B}) expected for

(30) Sokolowski, A.; Adam, B.; Weyhermüller, T.; Kikuchi, A.; Hildenbrand, K.; Schnepf, R.; Hildebrandt, P.; Bill, E.; Wieghardt, K. *Inorg. Chem.* **1997**, *36*, 3702.
(31) (a) Simándi, L. I.; Barna, T.; Argay, G.; Simándi, T. L. *Inorg. Chem.* **1995**, *34*, 6337. (b) Wicklund, P. A.; Beckmann, L. S.; Brown, D. G. *Inorg. Chem.* **1976**, *15*, 1996. (c) Adams, D. M.; Noodleman, L.; Hendrickson, D. N. *Inorg. Chem.* **1997**, *36*, 3966.
(32) (a) Duggan, D. M.; Hendrickson, D. N. *Inorg. Chem.* **1975**, *14*, 1944. (b) Brewer, G.; Sinn, E. *Inorg. Chem.* **1985**, *24*, 4580. (c) Tandon, S. S.; Thompson, L. K.; Bridson, J. N.; Dewan, J. C. *Inorg. Chem.* **1994**, *33*, 54. (d) Glerup, J.; Goodson, P. A.; Hodgson, D. J.; Michelsen, K. *Inorg. Chem.* **1995**, *34*, 6255.
(33) e.g. Pei, Y.; Journaux, Y.; Kahn, O.; Dei, A.; Gatteschi, D. *J. Chem. Soc., Chem. Commun.* **1986**, 1300. Pei, Y.; Journaux, Y.; Kahn, O. *Inorg. Chem.* **1988**, 399. Chaudhuri, P.; Winter, M.; Fleischhauer, P.; Haase, W.; Flörke, U.; Haupt, H.-J. *J. Chem. Soc., Chem. Commun.* **1990**, 1728.
(34) Earnshaw, A. *Introduction to Magnetochemistry*; Academic Press: London, 1968; pp 66−69. (b) Kahn, O. *Molecular Magnetism*; VCH: New York, 1993; p 8.

independent $S = 2$ Fe^{II} ($g = 2.0$) spins and is attributed to an effective g value of 2.08. Below 50 K, $\mu_{eff}(T)$ increases steeply to 8.20 μ_B at 6 K and then decreases rapidly to 7.39 μ_B at 2 K. Above 20 K, $\chi^{-1}(T)$ can be fit to the Curie−Weiss expression [$\chi \propto (T - \theta)^{-1}$] with $\theta = 1.7$ K, indicative of weak ferromagnetic interactions between the iron(II) ions. The data are modeled with the isotropic Fe(II) ($S = 2$) dimer spin Hamiltonian, H [$= -2J\mathbf{S}_1\cdot\mathbf{S}_2$], for which $\chi(T)$, eq 2, was derived. The best-fit parameters for $\mathbf{2}^{2+}$ to eq 2 are $g = 2.08$, $J/k_B = 1.0$ K (0.70 cm^{-1}), and $\theta = -1.1$ K.

$$\chi = [Ng^2\mu_B{}^2/3k_B(T-\theta)][6\exp(2J/k_BT) + 30\exp(6J/k_BT) + 84\exp(12J/k_BT) + 180\exp(20J/k_BT)]/[1 + 3\exp(2J/k_BT) + 5\exp(6J/k_BT) + 7\exp(12J/k_BT) + 9\exp(20J/k_BT)] \quad (2)$$

Hence, in contrast to $\mathbf{1}^{2+}$, $\mathbf{2}^{2+}$ exhibits a ferromagnetic interaction between the two Fe(II) ions via the CA^{2-}, even though with a long distance separation (ca. 8.06 Å). Note that $[Fe_2(CA^{2-})L_4](ClO_4)_4$ (L = Ph_2-Phen, Me_2-Phen, en, pn, ap) and $[Fe_2(CA^{2-})L_4](ClO_4)_4$ (L = bpy, phen, Me_2bpy, Me-phen, Cl-phen, NO_2-phen) that are expected to have the same structural core as that of $\mathbf{2}^{2+}$ exhibit antiferromagnetic interactions between the Fe(II) ions, i.e., $-2.08 > J > -8.65$ cm^{-1}.[35]

The room-temperature moment for $\mathbf{2}^{+}$ is 7.60 μ_B, and it increases gradually to 9.14 μ_B with decreasing temperature until 17 K, when it decreases rapidly to 7.63 μ_B at 2 K (Figure 6). The value of μ_{eff} at room temperature is larger than the value (7.14 μ_B) expected for independent $S = 2$ Fe^{II} ($g = 2.0$) spins, and this is attributed to $g_{eff} = 2.03$ and ferromagnetic coupling (vide infra). Above 17 K, $\chi^{-1}(T)$ can be fit to the Curie−Weiss expression with $\theta = 12.1$ K, indicating significant ferromagnetic interactions between the iron(II) ion and the radical of chloranilate. The data are modeled with the isotropic trimer spin Hamiltonian, H [$= -2J(\mathbf{S}_1\cdot\mathbf{S}_2 + \mathbf{S}_2\cdot\mathbf{S}_3)$], (Fe(II)−radical−Fe(II), $2{-}{}^1/_2{-}2$ system), for which $\chi(T)$, eq 3, was derived.

$$\chi = [Ng^2\mu_B{}^2/3k_B(T-\theta)][1.5\exp(4J/k_BT) + 1.5\exp(2J/k_BT) + 15\exp(5J/k_BT) + 15\exp(J/k_BT) + 52.5\exp(6J/k_BT) + 52.5 + 126\exp(7J/k_BT) + 247.5\exp(8J/k_BT)]/[2\exp(4J/k_BT) + 2\exp(2J/k_BT) + 4\exp(5J/k_BT) + 4\exp(J/k_BT) + 6\exp(6J/k_BT) + 6 + 8\exp(7J/k_BT) + 10\exp(8J/k_BT)] \quad (3)$$

The best-fit parameters to eq 3 for $\mathbf{2}^{+}$ are $g = 2.03$, $J/k_B = 28$ K (19.5 cm^{-1}), and $\theta = -2.2$ K. Thus, $\mathbf{2}^{+}$ shows a significant ferromagnetic interaction between Fe(II) and $CA^{\bullet 3-}$. The magnetic interaction (28 K) is much stronger than that (1.0 K) of $\mathbf{2}^{2+}$, indicating that the spin coupling occurs through $CA^{\bullet 3-}$. While both $\mathbf{2}^{+}$ and $\mathbf{2}^{2+}$ exhibit ferromagnetic coupling, J is 28 times greater for $\mathbf{2}^{+}$ again indicating that $CA^{\bullet 3-}$ is a stronger spin coupling group, as it couples via direct exchange (vide supra), than CA^{2-}, due to the overlap of the $CA^{\bullet 3-}$ π^* SOMO and the t_{2g} orbitals of Fe(II) ion that is not present for $\mathbf{2}^{2+}$.

The observation of ferromagnetic coupling is unexpected as related CA^{2-},[4a,36] oxalato,[32d,37] 2,2′-bipyrimidine,[32b] 1,2,4,5-tetrakis(benzimidazol-2-yl)benzene,[32c] and dicarboxylate[38] bridging dinuclear Co, Fe, Mn, Ni, and Cu complexes have been reported to exhibit antiferromagnetic coupling that ranges from −0.3 to −30 K. Likewise, $\mathbf{1}^{2+}$ exhibits weak antiferromagnetic coupling between cobalt(II) ions. Nonetheless, Fe-based $\mathbf{2}^{+}$ and $\mathbf{2}^{2+}$ display ferromagnetic coupling, but its genesis is not understood and requires further study.

Conclusion

A series of six dinuclear complexes of $[(TPyA)M^m(CA)M^m(TPyA)]^{n+}$ (M = Co, Fe, m = II, III, n = 1, 2, 3, 4) composition, namely, $[(TPyA)M^{II}(CA^{2-})M^{II}(TPyA)]^{2+}$ [M = Co($\mathbf{1}^{2+}$), Fe ($\mathbf{2}^{2+}$)], $[(TPyA)M^{II}(CA^{\bullet 3-})M^{II}(TPyA)]^{+}$ [M = Co($\mathbf{1}^{+}$), Fe ($\mathbf{2}^{+}$)], and $[(TPyA)Co^{III}(CA)Co^{III}(TPyA)]^{n+}$ [n = 3, CA = $CA^{\bullet 3-}$ ($\mathbf{1}^{3+}$), n = 4, CA = CA^{2-} ($\mathbf{1}^{4+}$)] have been prepared and characterized. The structures of $\mathbf{1}^{n+}$ (n = 1, 2, 3, 4) and $\mathbf{2}^{2+}$ reveal that all metal ions have a distorted octahedral geometry, and due to the interdimer offset face-to-face $\pi-\pi$ and/or herringbone interactions, the complexes display 1-D and/or 2-D supramolecular structures such as chain, layer, and ladder. Compounds $\mathbf{1}^{+}$, $\mathbf{1}^{3+}$, and $\mathbf{2}^{+}$ have the $CA^{\bullet 3-}$ trianion radical bridging ligand, and it occurs unexpectedly in valence ambiguous $\mathbf{1}^{3+}$. The existence of $CA^{\bullet 3-}$ is characterized by structural, solid-state magnetic susceptibility and solution EPR spectroscopy. Formation of $\mathbf{1}^{3+}$ occurs via a complex redox-induced electron rearrangement (RIER) whereby the one-electron oxidation of the $[Co^{II}CA^{2-}Co^{II}]^{2+}$ core forms $[Co^{III}CA^{\bullet 3-}Co^{III}]^{3+}$, not the expected simple $1e^-$ transfer mixed-valent $[Co^{II}CA^{2-}Co^{III}]^{3+}$ core. This type of reaction mechanism is rare but implicated in the NiFe-hydrogenases.[11] Furthermore, with respect to CA^{2-}, $CA^{\bullet 3-}$ enhances the spin coupling between the metal centers as shown in compounds $\mathbf{1}^{+}$ and $\mathbf{2}^{+}$, due to the direct spin exchange, and Co-based $\mathbf{1}^{2+}$ and $\mathbf{1}^{+}$ showed antiferromagnetic interactions, while Fe-based $\mathbf{2}^{2+}$ and $\mathbf{2}^{+}$ displayed ferromagnetic interactions.

Acknowledgment. We appreciate the helpful discussions with Paul W. Ayers (McMaster University), Eric L. Hegg, Roald Hoffmann (Cornell University), and Henry S. White and the continued partial support by the U.S. Department of Energy Division of Material Science (Grant No. DE-FG03-93ER45504 and DE-FG02-01ER45931) and U.S. Air Force Office of Scientific Research (Grant No. F49620-03-1-0175).

Note Added in Proof. Roald Hoffmann brought to our attention the paper entitled "Can one oxidize an atom by reducing the molecule that contains it?" by Paul W. Ayers where an orbital relaxation mechanism is invoked to achieve this phenomenon.[39]

Supporting Information Available: X-ray crystallographic data for $\mathbf{1}^{+}$ (CCDC#608644), $\mathbf{1}^{2+}$ (CCDC#608643), $\mathbf{1}^{3+}$ (CCDC#622484), $\mathbf{1}^{4+}$ (CCDC#622485), and $\mathbf{2}^{2+}$ (CCDC#622486) in CIF format. This material is available free of charge via the Internet at http://pubs.acs.org.

JA067208Q

(35) (a) Li, Y.-T.; Yan, C.-W. *Synth. React. Inorg. Met.-Org. Chem.* **1998**, *28*, 1283. (b) Li, Y.-T.; Yan, C.-W.; Zheng, Y.-J.; Liao, D.-Z. *Polyhedron* **1998**, *17*, 1423. (c) Li, Y.-T.; Yan, C.-W.; Zeng, X.-C. *Pol. J. Chem.* **1999**, *73*, 1673.
(36) (a) Tinti, F.; Verdaguer, M.; Kahn, O.; Savariault, J.-M. *Inorg. Chem.* **1987**, *26*, 2380. (b) Pierpont, C. G.; Francesconi, L. C.; Hendrickson, D. N. *Inorg. Chem.* **1977**, *16*, 2367. (c) Xiang, D. F.; Duan, C. Y.; Tan, X. S.; Liu, Y. J.; Tang, W. X. *Polyhedron* **1998**, *17*, 2647.
(37) (a) Rashid, S.; Turner, S. S.; Day, P.; Light, M. E.; Hursthouse, M. B. *Inorg. Chem.* **2000**, *39*, 2426. (b) Fuller, A. L.; Watkins, R. W.; Dunbar, K. R.; Prosvirin, A. V.; Arif, A. M.; Berreau, L. M. *Dalton Trans.* **2005**, 1891.
(38) Heinze, K.; Huttner, G.; Schober, P. *Eur. J. Inorg. Chem.* **1998**, 183.
(39) Ayers, P. W. *Phys. Chem. Chem. Phys.* **2006**, *8*, 3387.